

3-25-2012

# Interaction Between Electromagnetic Waves and Transport in Saturated Media

Mahsa Azad

*Boise State University*

Harlan Sangrey

*Boise State University*

Arvin Farid

*Boise State University*

Jim Browning

*Boise State University*

Elisa Barney Smith

*Boise State University*

# Interaction Between Electromagnetic Waves and Transport in Saturated Media

Mahsa Azad, Harlan D. O. Sangrey, Arvin Farid, Jim Browning, and Elisa Barney Smith  
Boise State University

## Abstract

Air sparging is one of the most popular remediation technologies. However, it is limited to a small radius of influence (ROI) surrounding the air injection well. Hence, there have been several efforts to improve its effectiveness. To study the possibility of improving the effectivity of air sparging electromagnetic (EM) waves, an easily visible analogous problem (dye transport in water) is studied in this paper. In order to quantify the effects of EM stimulation on flow of an inert, nonreactive dye in water, EM-stimulated and unstipulated dye transport experiments tests were performed and compared. To quantify this interaction, both dye transport and EM wave propoagation (only the electric field component Z) are quantified experimentally in lab-scale. In addition to the experimental mapping of the electric field at limited location on depth (i.e., vertical) slices, the electric field is simulated in COMSOL Multiphysics 4.1 in three dimensions (3D) for accurate field analysis. Transport analysis of the dye was performed using digital imaging to determine temporal and spatial concentration variations. The results show a visible effect on the dye transport mechanisms (i.e., fingering and diffusion). However, further study is needed to validate the proposed correlation between the electric field and the transport mechanisms.

**Keywords:** air sparging, remediation, electromagnetic stimulation, diffusion, viscous fingering

## Introduction

Environmentally hazardous spills of chemicals/petrochemicals and gasoline are serious concerns due to their potentially contaminating nature for groundwater. There is an increasing need for cleanup of these types of spills. This need is not expected to diminish in the foreseeable future, as large numbers of underground chemical/petrochemical and gasoline storage tanks around the country and world are aging and beginning to leak or have been leaking for years. The contamination due to these spills can seep into the ground, and without any treatment, the problem can spread to groundwater. If left untreated, the spill will take tens or hundreds of years to dilute and degrade to a level accepted by drinking water standards. The ability to treat large areas of spillage in an efficient and cost-effective manner is necessary for a feasibly faster treatment of contaminated sites. The ex-situ method of excavation and removal of contaminated soils is very expensive and destructive. Instead, there are several remediation technologies with different levels of effectiveness.

Air sparging is an increasingly popular method for remediation of sites contaminated with non-aqueous phase liquid (NAPL) spills. The method of pumping air into the contaminated groundwater is shown to be effective in reducing contamination via volatilization to acceptable levels. This method is a less invasive, yet effective, remediation process. It does, however, have limitations particularly due to its slow rate of cleanup. The air sparging process can take months or years and can, therefore, be very costly. This method is limited by random air channel formation (Elder and Benson, 1999), which creates a limited mass transfer zone (MTZ) between the medium and formed air channel (Braida and Ong, 2001).

One of the main existing methods to overcome air channel formation to enhance air sparging's effectiveness is pulsating. Pulsation attempts to alternate the location of formed air channels and is both time-consuming and uncontrolled. Vermeulen and McGee (2000) have examined electromagnetic (EM) bioheating and achieved promising result and enhanced the removal of volatile organic compounds (VOCs). However, only preliminary work was performed, and the process was not controlled. The generated heat enhanced airflow but can be harmful to unthermobolic bacteria. The use of in-situ heating was discussed without looking at the negative environmental

impacts due to overheating of the medium. There is also no study of the impact of the radio frequency (RF) stimulation other than heating.

### Scope

This work focuses on the main goal of using electromagnetic (EM) stimulation to expedite air sparging without any considerable/measurable temperature increase. The main motivation behind selection of EM stimulation is to demonstrate that the frequency of EM waves can be controlled to reduce the generated heat to maintain the temperature of the medium while simultaneously stimulating the airflow.

The first step is to determine the effects of EM stimulation on diffusion. It is based on the hypothesis that the stimulation of the saturated medium expedites diffusion and that a relationship between diffusion rate to different frequencies and power levels of EM stimulation can be correlated.

As the first step, instead of airflow in saturated soils, an analogous problem (dye diffusion in water) is studied in the laboratory. The diffusion of a nonreactive dye in water was used as a visible analogy to air sparging in saturated soil. When a nonreactive, inert dye is introduced in water, fingers of dye will be formed and around and within these fingers, diffusion is the main mechanism controlling the transport and distributing the dye. The results are analyzed quantitatively. The Electric field was simulated in COMSOL Multiphysics to provide a numerical model for this experiment to achieve the 3D vector, complex, electric field. The experiment is performed in a Faraday cage (184 cm × 163 cm × 138 cm) to create a controlled boundary condition for the EM wave propagation and protect laboratory users from any possible harm (Jamieson et al., 2007). However, the large size of Faraday cage, the orientation and position of the antenna should be refined to lower the computational cost of the numerical modeling in the future.

### Materials and Methods

**Summary of Test Method:** EM-stimulated tests are performed in a 40 cm × 40 cm × 40 cm clear acrylic cube using a submerged monopole antenna as the source of EM waves. The monopole antenna is an N-type RG8 coaxial cable with 70 mm of the conducting shield stripped, placed in a CPVC casing, and submerged in the medium. The antenna and CPVC casing are bent in an L-shape to avoid drilling any opening in the vertical walls of the acrylic box. The CPVC pipes, table, and acrylic box are shown in Figure 1.

A CW (continuous wave) RF signal is generated using an HP E4400B signal generator. A Model 100 LMB amplifier manufactured by Amplifier Research is used to amplify the generated signal. To maximize the power output and reduce reflection back into the amplifier, a matching network is used to match the impedance of the medium to the one of the amplifier (50Ω); the source impedance. The matching network includes two 14 pF – 380 pF variable two-gang capacitors, one in parallel, and one in series to tune the impedance of the testing medium. To measure the circuit impedance for network matching, the system (i.e., the antenna submerged in the medium, the cables, and the matching network) is connected to an Agilent Technologies E5071C vector network analyzer (VNA). As seen in Figure 2, the entire system is placed in a large Faraday cage. A wooden frame with an aluminum screen stretched across is assembled and carefully grounded with a removable door for access to create a uniformly conducting cage, although the door was not used during testing.

De-ionized, de-aerated water is used for all the tests. Using the de-aerated water is very important to prevent generation of air bubbles in order to acquire clean images of the dye for analysis.

Using a pipette, the dye is delivered to the center of the acrylic injection table in the water tank for both stimulated and unstimulated tests. The dye is injected into a concave depression ground on top of an acrylic table. This table allows the dye to be introduced to the middle of the test medium without immediately flowing away. For dye injection, a syringe is used to inject a carefully measured amount of dye (1.2 g) into the pipette.

The electric field is mapped in the test region using a three dimensional computer controlled translation table. The table is used to move a probe connected to the spectrum analyzer to points of any desired 3D grid. The three-axis positioner was built using an aluminum frame, stepper motors, and ball screws for positioning. The mechanical and electrical components were designed and were built in house.

Digital imaging is used to analyze the transport of the dye. Taking images at consistent time intervals and using the images to measure dye concentrations, enables the determination of the transport rate. The lighting of the test medium is very important to the analysis of the diffusion. To ensure a uniformly lit background, a light box is built along with a diffusive filter. The light box consists of a wooden frame built out of fir attached to a plywood backing. Three florescent tube lights are attached to the inside and back of the box. To diffuse the light, white Lycra is stretched across the opening of the box. To diffuse the light further and to create a more uniform backlight for the apparatus, a second frame made with white Lycra is used. These two layers of Lycra are spaced approximately 20 cm apart to diffuse the light enough to reduce drastic backlight gradients to an acceptable level.

Before the dye injection, ten images are taken and averaged to represent the background. This averaged background image is subtracted from all other remaining images. Once the background has been subtracted, leaving just the dye in the images, analysis of the dye can begin. Series of images of various fully-diffused dye concentrations are taken to calibrate the concentration of the dye to the image pixel-intensity. Calibration images are taken with known time increment, and hence, known incremental increases of concentration and used to calibrate the concentration in the stimulated and unstimulated diffusion tests. A relationship between concentration and pixel value is established for a range of concentrations, but any pixel values above the calibrated concentrations are given the maximum calibrated value. This point of extremely high dye concentration exists only within dye fingers. Assigning the maximum calibrated value will affect the results but mostly within the formed dye fingers.

The images were separated into the three light spectra (i.e., red, blue, and green). The calibration factor would also be different for different colors of red, blue, and green, as well as spatially. The calibration factors are specific to the lighting of this experiment and needs to be evaluated, if the experiments are replicated under a different lighting condition. The red and blue channels will be used to measure the dye concentration in this analysis because their intensity better correlated to the dye concentration and only the results for blue is demonstrated in here.

**Simulation:** For a complex, full vector, 3D visualization of the electric field, the Faraday cage, the acrylic cube with the water inside and the coaxial antenna were modeled in COMSOL Multiphysics 4.1 (Figure 3). However, the electric field produced was not consistent with the experimental field measured in some aspects. It should be mentioned that the flow and diffusion were not modeled and only the electric field was simulated.

The antenna body could not be simulated exactly which might slightly affect the results. Also, because the Faraday cage was large in size, the equipment that were placed inside the cage such as the extended part of the antenna body to reach the top boundary of the cage (and from there to the electrical components) and antenna positioning table used for measuring the field may have affected the experimentally field measurements. These details could not be simulated in the model, which justifies the discrepancies between the experimental and simulated electric field measurements. A better controlled cavity structure is being used to eliminate these issues in the ongoing work (not mentioned in this paper).

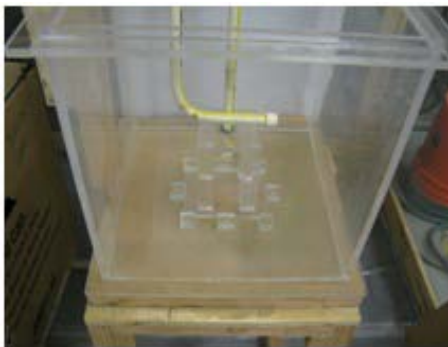


**Figure 1. Acrylic test box, dye injection table and CPVC antenna case.**

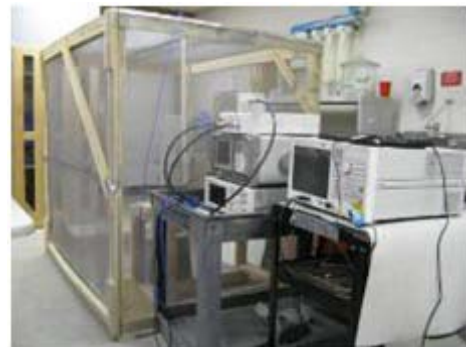


**Figure 2. Setup and devices used for EM stimulation tests.**

## Results and Discussions

**Diffusion Coefficient ( $D$ ) for Unstimulated Tests:** The diffusion without EM stimulation is fairly radially symmetric about the injection area. Figure 4 shows the unstimulated diffusion pattern where the dye descends vertically from the injection table and randomly spreads in all directions along the bottom of the tank and up the sides. Even though the problem is three dimensional, but since images are two dimensional (i.e., the intensity of each image pixel correlates to the integral of the concentration of the dye along the line of sight corresponding to the pixel). The camera is placed at a distance far enough from the test box in a way that line of sights of the central region (away from boundaries) of the box are relatively parallel. Therefore, the problem is studied as a 2D problem.

A finite difference (FD) code was written in Matlab to calculate the diffusion coefficient based on the Fick's second law. The Fick's second law for a homogenous and isotropic medium (i.e.,  $D_x = D_z = D$  and spatially constant) is as follows.

$$\frac{\partial C}{\partial t} = D \left[ \frac{\partial^2 C}{\partial x^2} + \frac{\partial^2 C}{\partial z^2} \right] \quad (1)$$

where  $C$  is concentration ( $\text{mol/m}^3$ ),  $t$  is time (s),  $D$  is the diffusion coefficient ( $\text{m}^2/\text{s}$ ), and  $x$  and  $z$  are coordinates (m) shown in Figure 3.

The results from the digital pixel analysis provide a matrix of concentration of 208 nodes at 130 time steps. The nodes are spaced every 2 cm. Images are saved at 1 minute time intervals. Equation (1) uses an implicit discretized backward difference in time and second order backward then forward difference consecutives in space to acquire a stable result as follows.

$$\frac{C_{x,z}^m - C_{x,z}^{m-1}}{dt} = D \left[ \frac{C_{x-1,z}^m - 2C_{x,z}^m + C_{x+1,z}^m}{(dx)^2} + \frac{C_{x,z-1}^m - 2C_{x,z}^m + C_{x,z+1}^m}{(dz)^2} \right] \quad (2)$$

Due to the assumption of homogeneity and isotropicness,  $D$  can readily be calculated for each node, and the system of equations does not need to be solved simultaneously. Then, Equation (2) was used for two unstimulated tests to find  $D$ . Based on this equation, a matrix was produced giving the diffusion coefficient for 154 nodes ( $D$  was not calculated for boundary nodes) at 129 times. There are areas where dye fingers rapidly move in and out. On the other hand, diffusion is the governing mechanism. Hence, consecutive digital images need to be inspected and  $D$  should be computed for the nodes where diffusion occurs (outside or within stable fingers within the consecutive time steps). The common range of diffusion coefficient for a liquid in water is  $10^{-4}$ - $10^{-6}$ . If attention is not paid to this fact, and simple averaging is performed over the entire region, an average diffusion coefficient over time and

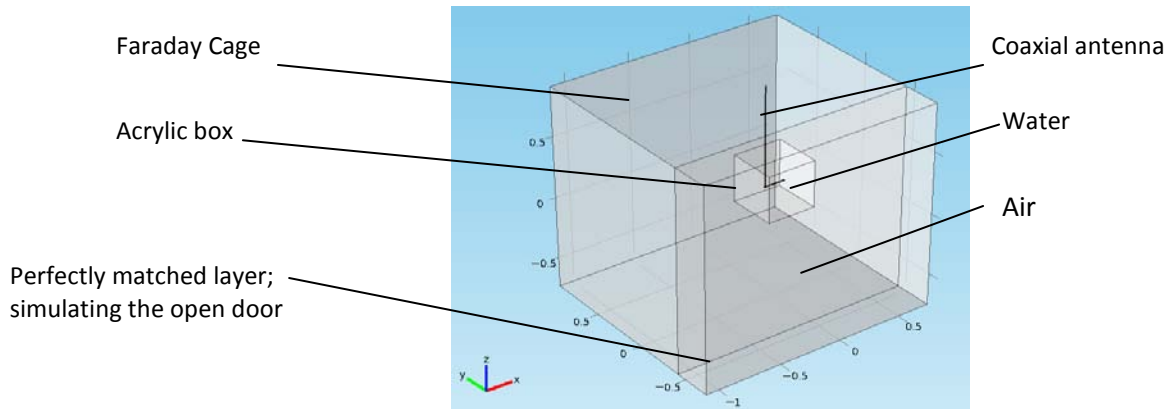


**Figure 3. Simulated Model for EM Stimulation tests.**

space and two runs of the test will be 0.056 for 0 Watts of power. This is too large for liquid in liquid diffusion. In other words, the transport mechanism is not diffusion over the entire space.

A more detailed study on the unstimulated tests shows that the fingering of dye during diffusion almost never stops. This phenomenon occurs everywhere in the acrylic box during the transfer mechanism. Nevertheless, inspecting the concentration of the dye at specific nodes and times with an acceptable value of  $D$  ( $10^{-4}$  -  $10^{-6}$ ) confirms the previous hypothesis about diffusion and fingering zones and provides interesting results. Reasonable values of  $D$  or in other words diffusion occur either when the concentration is low or where the node is located in stable fingering area. In the former situation, the node is located far from the fingering area, and therefore, diffusion can take place whereas in the latter case, the diffusion is indeed happening in the fingering region.

**Stimulation:** The antenna was originally positioned vertically in the vertical CPVC casing in the box. The EM-stimulation from the vertically polarized antenna created a focused transport pattern very similar to a vertical convective flow towards the antenna. To ensure that the heat generated surrounding the antennas has not created a convective flow, the temperature of the water was monitored. No measureable temperature change was observed and confirmed that there was no convective flow. This was a sign of the effect of the radiation pattern on the flow. To confirm this and to evaluate the effect of the radiation pattern of the stimulating electric field, the antenna was placed horizontally. The horizontal antenna created a very consistent effect that was easily captured with digital imaging. Figure 5 shows the flow of the dye to the right of the testing medium with very little dye flowing to the left. The contrast in the flow pattern shows the clear effect of the EM stimulation and radiation pattern of the antenna on the transport of the dye in water. The tests were repeated and showed strong consistency. These series of tests clearly verify the effect of the EM-stimulation and radiation pattern on the dye transport. The results of the following tests were all obtained with a horizontally-polarized antenna. There were four series of tests at 50 Watts, 30 Watts, 10 Watts, and 0 Watts, consisting of two replicas for each, at a frequency of 154 MHz.

The electric field probing technique enables construction of a map of the RF electric field and antenna radiation pattern using Lab View software. The output will be saved into an ASCII format comprised of the electric field measurements on a 4-column tab-delimited file representing the Cartesian coordinates of each probing point (X, Y, and Z) and the corresponding power reading (dBm), respectively. Figure 6a shows a schematic of the location of ten selected depth slices of the medium that the probing has been performed on. The power data is converted to a linear scale. The electric field maps are normalized to the global maximum and minimum values measured throughout the entire collected data. The normalization of the data is necessary to maintain the same relative scale in order for the comparison between the experimentally collected and simulated electric fields. Figures 6b and 6c show the experimental and simulated map of a sample of the 10 contour maps of the electric field amplitude on the corresponding depth slices described in Figure 6a. Due to the vertical polarization of the monopole probe (i.e., the vertical orientation of the probe) used in laboratory for measuring the electric field, it is believed that the measured field values are representing the Z component of the electric field. Therefore, the measured field is compared with  $E_z$  from the simulation.

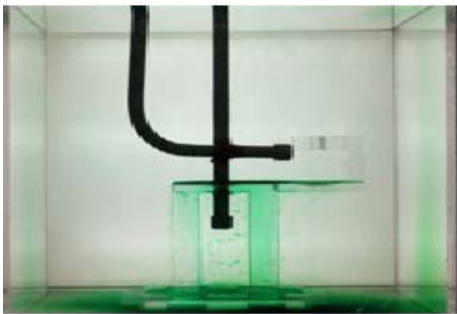


**Figure 4. Unstimulated Diffusion Pattern.**



**Figure 5. Stimulation with Horizontally Polarized Monopole Antenna.**

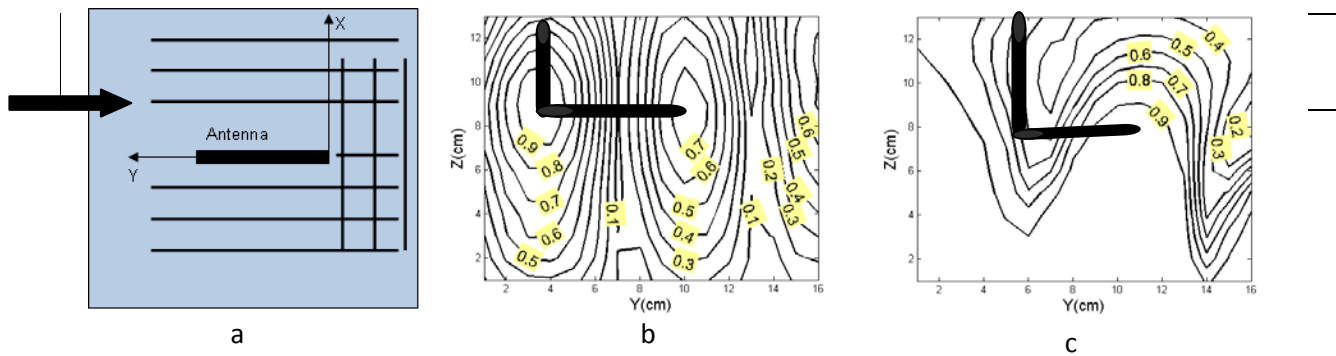


**Figure 6. (a): Schematic of field mapping depth slices locations (top view of setup); a depth slice parallel to the antenna spaced 8 cm from center to the back of the box is specified; (b) normalized electric field map ( $E_z$ ) from simulation by COMSOL Multiphysics on the specified slice in (a); (c) normalized electric field map ( $E$ ) measured using a vertically (Z-axis) polarized from experimental data on the specified slice in (a).**

test.

test.

In all the measured field maps, the highest intensity of the electric field is toward the left and bottom of the tank. The reason is not completely understood. Also, for slices perpendicular to the antenna direction, as the probing distance from the antenna increases from 2 cm to 6 cm and then to 10 cm, the intensity of the field decreases, but not as much as expected with a propagating wave. With a standing wave pattern, the field does not decrease radially away from the antenna. A standing wave pattern is visible in the field maps, corresponding to the wavelength of the RF wave in the medium. The Faraday cage most likely causes this standing wave pattern instead of the propagating wave that might otherwise be expected.

On the other hand in every other simulated field maps, the highest intensity of the electric field occurs toward the left (horizontally) and middle (vertically) of the tank where the vertical portion of the antenna body exists. This can be explained through the fact that the outer conductor of the coaxial cable is located in that portion of the box.

The difference in the two field maps can be explained through the fact that not all details such as the translation table of the experiment could be modeled. Due to this difference, the concentration will be correlated to the experimental measurements for now and this paper.

**EM Stimulation Effects:** A MATLAB code (m-file format) was developed to quantify and analyze dye movement. The program integrates the amount of dye in different zones of the medium. The five zones that are used for comparison to determine the effect of the EM stimulation are shown in Figure 7. To quantify the tendency of the dye to flow toward the right side of the testing box during EM-stimulation and compare it with no apparent preferred path in unstimulated tests, Zones 2 and 4 are compared.

In Figure 8, Zone 2 concentration, 50W-Z2R1, diverges from the Zone 4 concentration, 50W-Z4R1. 50W-Z4R1 is the notation for 50-watt stimulated test, Zone 4, and the number 1 indicates that this was Run 1 out of 2 diffusion

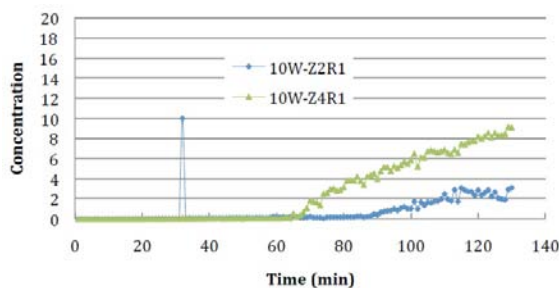


**Figure 10. Zones 4 and 2, diverging concentrations in 10-Watt stimulated test.**

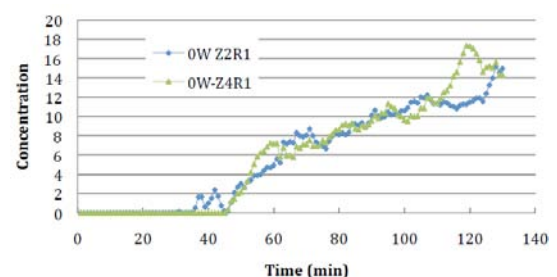


**Figure 11. Zones 4 and 2, diverging concentrations in unstimulated test.**

tests performed for 50-watt stimulation. The tests shown in Figures 8 through 11 are all of the same imaging Zones 2 and 4, during stimulation at 50, 30, 10 and 0 Watts at 154 MHz.

The slope of the concentration versus time is a representative of the rate of increase in concentration in Zone 4 relative to Zone 2 and, therefore, is proportional to the rate of relative transport (transport flux) of the dye.

Another approach for correlating concentration to electric field was observing the change of concentrations of nodes along the contour line of the electric field map in comparison to nodes on a line normal to the same contour line. If the concentration is related to the electric field intensities, the change of concentrations over time of nodes along the electric field contour line should be different from the nodes normal to that contour-line. Figure 12 shows one example of the results of this approach for nodes 'a' and 'd' along a contour line and 'b' and 'c' normal to that contour line. For some sets of nodes as the one brought here, the difference is greater for nodes normal to a contour line, however the opposite occurs for other sets of nodes. Therefore, the correlations of the transport mechanism to the electric field are more complicated. As seen in Figure 12 at 30 watts of power, the behavior seems as random as the unstimulated tests.

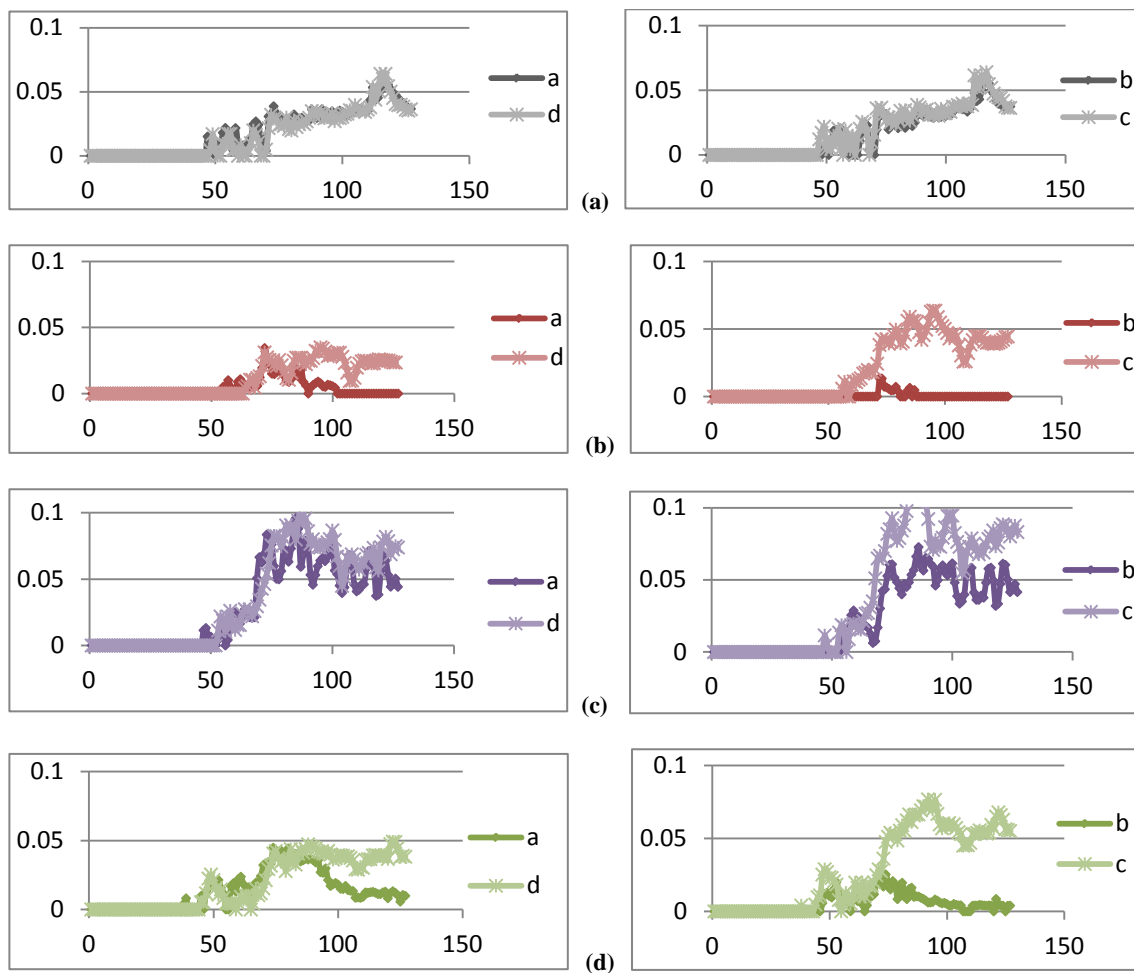


**Figure 12. Change of Concentration over time for (a) 0-Watts, (b) 10-watts, (c) 30 watts, (d) 50-Watts. 'a' and 'd' are nodes tangential to the electric field lines, 'b' and 'c' are normal to electric field lines.**



## **Conclusion**

This research is the initial stage and the first step in the investigation of the effect of EM stimulation on air sparging. The data clearly shows that EM stimulation affects the transport of the inert, nonreactive dye in water. The ability to create a relationship between the stimulation power (and hence electric field) and transport rates requires more analysis. Understanding and mapping the field will help to clarify the mechanisms occurring in the stimulated medium. The biggest improvement to the testing apparatus and procedure would be to employ a proper antenna design to create an easier more compatible method to theoretically model the EM-field and make computation and development of a correlation between the electric field and dye transport easier. Also, a smaller Faraday cage (or even a resonant cavity) will show the full potential of this research. To better investigate the effect of stimulation, a better visual picture of unstimulated transport mechanism is required. More detailed studies on decoupling diffusion and fingering is needed to understand the movement mechanism before and after EM stimulation.

There is not enough evidence to demonstrate that the governing flow mechanism is dielectrophoresis or dielectrophoresis mixed with any other flow mechanism (e.g., diffusion). A better field pattern would make this judgment more feasible.

## **Acknowledgements**

This project is supported by the National Science Foundation IDR program (CBET Award No.0928703). The authors would like to express appreciation toward Carco Mineral Resources Inc. for donating the bentonite, Harlan Sangrey and The Boise State University Instrumentation Section for fabrication and machining support with the permeameters.

## References

- Braida, W., and Ong, S. K. (2001). "Air sparging effectiveness: laboratory characterization of air-channel mass transfer zone for VOC volatilization," *Journal of Hazardous Materials*, B87, pp. 241-258.
- Crank, J. (1975), "The Mathematics of Diffusion", Second edition.
- Elder, C., and Benson, C. H. (1999). "Air channel formation, size, and spacing, and tortuosity during air sparging," *Ground Water Monitoring & Remediation*, pp. 171-181.
- Falta, R. W. (2001). *Steam flooding for environmental remediation, Manuals and Reports on Engineering Practice*, American Society of Civil Engineers (ASCE) 0734-7685, Vol. 100, pp.153 .
- Fick, A. (1855), On liquid diffusion, *Philosophical Magazine and Journal of Science*, (10), 31-39
- Price, S. L., Kasevich, R. S., Johnson, M. A., Wilberg, D., and Marley, M. C. (1999). "Radio Frequency heating for Soil Remediation," *Journal of the Air and Waste Management Association*, Vol. 49, pp. 136-145.
- Tsai, Y. (2007) "Airflow paths and porosity/permeability change in a saturated zone during in situ air sparging" *Journal of Hazardous Materials*, Vol. 142, pp. 315-323.